Experimental measurement of energy release from an initiating layer in an insensitive explosive

Eric K. Anderson*, Carlos Chiquete, Scott I. Jackson

Shock and Detonation Physics Group,
Explosive Science and Shock Physics Division,
Los Alamos National Laboratory, Los Alamos, NM 87545 USA

Abstract

When subjected to a shock of insufficient strength to trigger prompt reaction, heterogenous condensed phase explosives can form regions where significant amounts of the explosive remain unreacted for times much greater than the reaction time of the detonating explosive. This phenomena is observed for the explosive PBX 9502 (95 wt% TATB) both for planar and oblique input shocks. In this work, we build on previous results by performing cylinder expansion (CYLEX) tests where the explosive charge is comprised of a faster core of PBX 9501 (95 wt% HMX) inside a slower annulus of PBX 9502. The detonation in the faster PBX 9501 drives an oblique shock into the adjacent PBX 9502, and an annular transverse initiating layer (IL) results. In the test geometry, the IL travels steadily down the length of the test after a short run distance. At radial positions beyond the IL, an annular region of detonating PBX 9502 is observed. Using standard CYLEX test diagnostics, we infer the total energy release of this experiment. By making the assumptions that (1) the combined energy release is comprised of contributions from detonating PBX 9501, detonating PBX 9502, and the IL in the PBX 9502 and (2) mass-specific energy release for the detonating explosives is approximately the same as typically observed for each explosive, the IL energy release and reaction efficiency can be computed. Results are compared to prior results for a similar geometry, and indicate that while shock deadened PBX 9502 does not detonate promptly, it does eventually release a significant portion of its chemical potential energy over longer timescales on the order of $10\,\mu$s.

Keywords:
Detonation, Cylinder Test, Dead Zone, Initiation Layer

*Corresponding author:
Email address:* eanderson@lanl.gov (Eric K. Anderson)

1. Introduction

Driving an oblique shock into the surface of an explosive can produce a region in the explosive where prompt detonation does not occur. This region has been called a dead zone [1] and in certain configurations an initiating layer (IL) [1, 2]. The term IL applies to regions where detonation does not occur, but energy is released at a slower rate. In addition, this energy appears to contribute to a turn-over to detonation in the explosive beyond the IL. This phenomena has been shown to be analogous to the 1-D shock to detonation transition [2] which has been well characterized for many explosives in wedge-tests and gas-gun experiments [3–5].

An oblique shock capable of producing an IL can be generated by detonating a faster explosive adjacent to the explosive where the IL is to be formed. An example is shown Fig. 1, where an IL is visible in a radiograph taken during an experiment where detonating PBX 9404 (94 wt% HMX, 3 wt% tris-β chloroethylphosphate (CEF) plasticizer, 2.9 wt% nitrocellulose (NC), and 0.1 wt% diphenylamine (DPA)) drives an oblique shock into adjacent X0237 (90% TATB, 5% wax, and 5% Elvax).
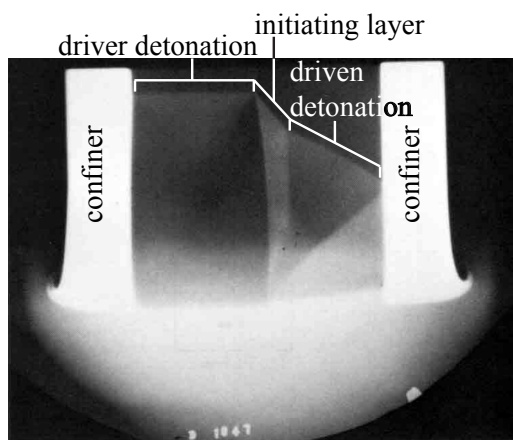

Figure 1: Flash X-ray image of PBX 9404 shocking X0237 obliquely, with the detonation traveling from the bottom to the top of the image. D. Venable, Shot 1047, LANL 1969 [6].

Previous studies of ILs in TATB-based explosives have been conducted in the slab geometry [2, 6–9] as well as the cylindrical geometry [1, 10]. The cylinder expansion (CYLEX) test is a particular cylindrical geometry where a cylinder of explosive is placed inside a confiner tube of precision machined, high purity, dead soft copper in order to measure the wall motion of the confiner. The wall motion can be analyzed to determine the product equation of state and to quantify the energy generated by detonation of the explosive. Hill [1] performed a CYLEX test where the explosive charge was a 14.0 mm diameter cylinder of PBX 9501 inside a shell of PBX 9502 with an inner diameter (ID) of 14.0 mm and outer diameter (OD) of 25.4 mm. In this geometry, the PBX 9501 detonation will run ahead of the PBX 9502 and transversely initiate the PBX 9502 shell. A steady wave structure is formed with detonating PBX 9501 at the center, an IL in the PBX 9502 immediately adjacent to the PBX 9501, and detonating PBX 9502 outside the IL.

Hill measured the detonation wave speed, shape of the breakout at the downstream end of the test, and wall motion of the confiner. Using these measurements, the cross sectional areas of detonating explosive and IL were determined. By comparing the energy of the annular test to energy measured in single explosive CYLEX tests for PBX 9501 and PBX 9502, the energy release of the IL was inferred.

This paper describes the results of two additional annular CYLEX tests. The first consisted of a 13.5 mm PBX 9501 core inside a PBX 9502 annular shell, and in the second test a 14.5 mm core was used. These core dimensions were chosen to bracket that of [1]. We analyze these tests in a process similar to the one described in [1] and compare the inferred reaction efficiency of the IL in each of the tests. Our results indicate that the IL does react to release a significant amount of energy and that the magnitude of energy release varies with the IL shock strength.

2. Experimental Design

Two CYLEX tests were fielded for this study; the explosive charge in the first was a 13.5 mm diameter PBX 9501 core inside a PBX 9502 shell, while the second test utilized a 14.5 mm diameter PBX 9501 core inside a PBX 9502 shell. Examples of the parts are shown in Fig. 2. The outer diameter of the PBX 9502 and confiner length, inner diameter, and outer diameter were nominally standard CYLEX test dimensions of 25.4 mm for the PBX 9502 OD and the confiner ID, 30.48 mm confiner OD, and 304.8 mm length. The confiner measurements taken at the PDV probe measurement locations are listed in Table 1. The confiner tubes were prepared using oxygen-free high-conductivity (OFHC) copper and annealed dead soft. The explosive parts were all 25.4 mm long, and the bore of the PBX 9502 shell was slightly smaller than the diameter of the PBX 9501 core before the parts were pressed together, resulting in

2

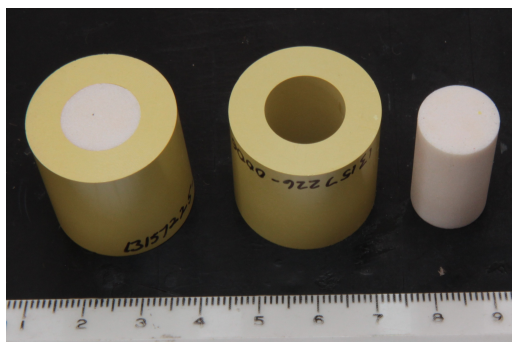a final assembly with no gaps between the two explosives.

Figure 2: PBX 9502 shell with pressed in PBX 9501 core (left), PBX 9502 shell (center), and PBX 9501 core (right). The scale at the bottom is in cm.

Table 1: Test dimensions and densities for shots 8-2047 (13.5 mm core) and 8-2048 (14.5 mm core).

Core Diameter (mm)	PBX 9501 Density (g/cc)	PBX 9502 Density (g/cc)	Confiner ID (mm)	Confiner OD (mm)
13.5	1.835	1.892	25.474	30.503
14.5	1.835	1.892	25.471	30.522

The 25.4 mm long cylinders of PBX 9501 and PBX 9502 were installed in the confiner with degassed Sylgard 184 mixed with DOWSIL 3-6559 cure accelerator in the recommended ratio. After curing, each test was instrumented with 11 shorting wires placed in a line on the outer surface of the confiner tube, in order to measure detonation velocity. Confiner wall motion was measured at 8 positions for each test using photon Doppler velocimetry (PDV) probes aligned normal to the tube wall surface. Finally, the detonation front shape was measured using a mirror destruct technique with a Cordin 132 streak camera. An image of the window for streak camera imaging is shown in Fig. 3. Illumination was provided with an explosively driven argon flash [11]. A test assembly is shown in Fig. 4.

3. Modeling

Multimaterial hydrodynamic simulations were employed to analyze the complex wave structure produced by the layered high explosive (HE) design of our experiments, and help qualitatively explain the experimentally measured confiner wall velocity profiles described in §4. This required a definition of constitutive models for the two HEs and the copper confiner. For PBX
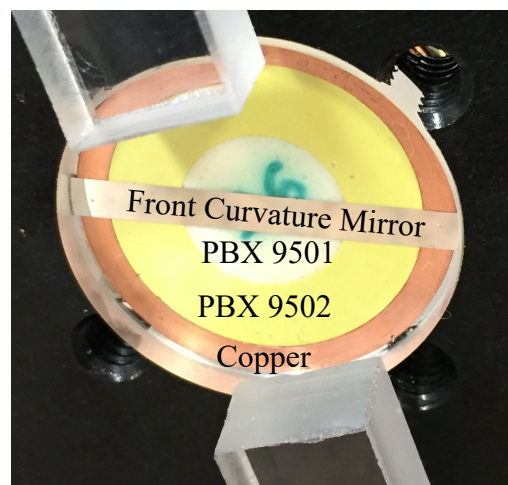

Figure 3: Close-up of the streak camera window showing PBX 9502 shell (yellow) and PBX 9501 core (white) for shot 8-2047.
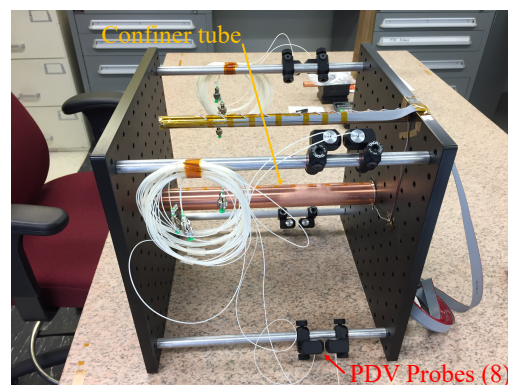

Figure 4: Assembly photograph of shot 8-2047.

9502, a modified Wescott-Stewart-Davis (WSD) reactive flow model [16] was used. The modifications to the model and specific model parameters are described in [17]. Informed by the initiating layer thickness determined from the experiment, the PBX 9502 material was split into two regions. The initiating layer was populated with the same EOS and reaction rate parameters as in the pristine region with one exception, the reaction was cutoff at 50% completion in order to mimic the partial energy release using an approximately average value suggested by our analysis of the initial 6 μs of the experimental wall motion. Secondly, for PBX 9501, a similar modified WSD model was used. This particular model was calibrated to recent 2D planar geometry tests (or "slabs") and described in [18]. Finally, the inert confining copper material was modeled using a tab-

3

ular equation-of-state detailed in [19] and its plastic deformation under shock loading was modeled according to [20]. The simulations were performed in the multiphysics, multimaterial Lagrangian hydrodynamics code Flag [21, 22]. For the results presented here, a fixed 62.5 μm resolution was used, which resulted in a converged wall motion profile. This resolution and the chosen 50% reaction completion may be further optimized, but are nevertheless sufficient to provide possible physical explanations for the experimentally observed wall motion.

4. Experimental Results

4.1. Detonation Velocity and Front Shape

For each test, the shorting wires measure the speed of the lead shock wave as it travels down the length of the confiner. The measurement is performed by monitoring the voltage on the confiner while the shorting wires are held at approximately 75 V during the test. The result is a voltage spike when the insulation on each wire is crushed by the shock wave. Assuming the test is steady, the measured wire signals are fitted to a line and the slope is taken to be the detonation phase velocity, D_0. Measured values for both tests are reported in Table 2. For both tests, the standard error associated with this fit was approximately 0.004 mm/μs.

Measured front shapes for the two annular CYLEX tests are shown in Fig. 5. To compute the IL angle, we performed separate linear fits to the IL and detonating PBX 9502 on each side of the scaled front shape for each experiment. The intersection of the fitted lines was taken to be the outer extent of the IL, while the inside of the IL was taken to be the interface between the PBX 9501 and PBX 9502. The normal shock speed U_{IL} was then computed using D_0 and the IL angle, ϕ, as defined in Fig. 5. The IL shock pressure is computed using the method described in [2], with a Mie-Grüneisen Keane equation of state (EOS) for unreacted PBX 9502.

Figure 5: Scaled front shapes for the test with the 13.5 mm PBX 9501 core (blue) and 14.5 mm PBX 9501 core (red) Regions 1, 2*, and 2 represent the PBX 9501, PBX 9502 IL, and detonating PBX 9502 for the 13.5 mm core test.

Table 2: Results for shots 8-2047 (13.5 mm core) and 8-2048 (14.5 mm core).

Core Diameter (mm)	13.5	14.5
D_0 (mm/μs)	8.791	8.818
Average IL Angle (°)	48.389	47.064
Normal IL Shock Velocity (mm/μs)	5.838	5.988
IL Shock Pressure (GPa)	19.356	21.095
PBX 9502 Detonation Angle (°)	26.619	29.920

4.2. Confiner Wall Motion

For each test, wall velocity profiles recorded using PDV were averaged separately for locations at axial positions of 2/3 and 3/4 run distance. The resulting averaged profiles are shown in Fig. 6 for both tests. The velocity profiles are quite different qualitatively from the ringing profiles observed in single explosive CYLEX tests [12].
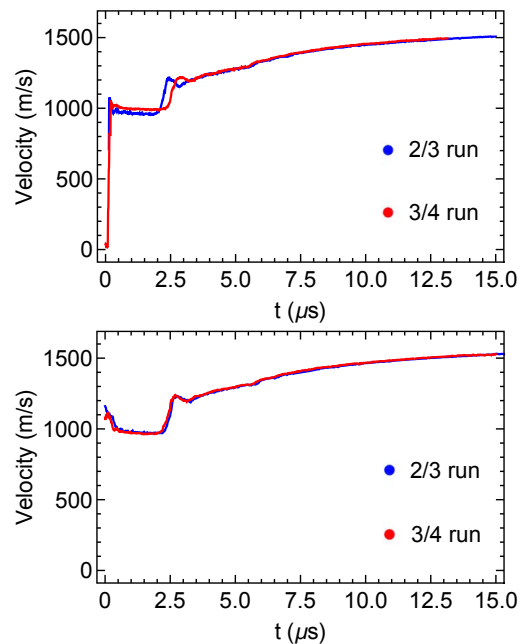

Figure 6: Confiner wall velocity profiles for tests with the 13.5 mm PBX 9501 core (top) and 14.5 mm PBX 9501 core (bottom).

In both tests, the wall motion exhibits three compressible features before becoming incompressible [12]. The first motion of Fig. 6 is a shock associated with the wave driven through the copper by the detonating PBX 9502 layer, as indicated by the dashed line at $t = 0$ in Fig. 7. We hypothesize that, following this first motion, the confiner has spalled in the radial direction, with the outer confiner surface decoupled from its inner surface. This results in the near steady velocity observed by the

PDV probes between approximately 0.5 μs and 2 μs, as shown in Fig. 6. Spall is not modeled in the simulation results of Fig. 7, but the simulation does indicate negative pressures in the confiner wall in excess of the copper tensile strength following first motion, which supports the spall hypothesis. The modeling of this test was performed to help understand the wave structure in the HE, and its impact on confiner motion.

The second compressible feature is visible in Fig. 6 around 2.5-3.0 μs after jump. The presence of this feature suggests that the copper confiner has recollected at this time and is again accelerated outward. The timing of this jump corresponds roughly to the third ring of the simulation results shown in Fig. 7. Following this acceleration, a gradual deceleration is visible for approximately 0.5 μs, suggesting that the confiner has again decoupled in the radial direction. Interestingly, the arrival of the second compressible feature is delayed at the 3/4 run position for the test with the 13.5 mm core. This delay is consistent across all probes, suggesting the flow is not fully steady at the 2/3 measurement location. This apparent unsteadiness is not observed for the test with the 14.5 mm core.

Following this feature, from approximately 4-5.5 μs after jump, the confiner appears to accelerate in an incompressible fashion until a third, small compressible feature appears just before 6 μs after jump. This feature correlates approximately with the shockwave visible in Fig. 7 that originates at the PBX 9502 detonation-IL interface, merges with a shock traveling inward from the PBX 9502-confiner wall interface, and then travels inward to the centerline of the experiment where the waves converge and reflect outward again to reach the confiner at approximately 6 μs after jump.

5. Analysis

To determine the reaction efficiency of the IL, we compute the mass fraction of the PBX 9501, detonating PBX 9502, and IL relative to the total explosive mass for each test. Cylinder kinetic energy (CE) is computed for each concentric test as a function of time after first wall motion. We then use mass-specific CE values from previously reported PBX 9501 and PBX 9502 cylinder tests to compute the CE contribution from the PBX 9501 and detonating PBX 9502 in the concentric tests. These CE values are also computed as a function of time after first wall motion. With the total, time-varying CE for each concentric test and the time-varying contributions from the detonating PBX 9501 and PBX 9502 determined, the CE contribution from the PBX 9502 IL can
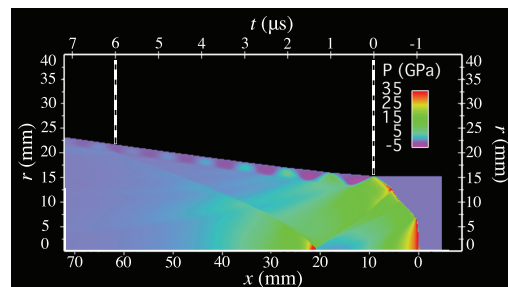

Figure 7: Pressure field generated by hydrocode simulation of the annular test with the 13.5 mm core. In this figure, the vertical axes represent distance from the experiment centerline, the upper horizontal axis shows time relative to first wall motion, and the lower horizontal axis shows distance relative to the lead shock in the detonating PBX 9501. Details of the simulation are described in §3.

be computed as a function of time after first wall motion. Our approach is similar to the energy analysis of [1] with several modifications:

1. We account for the effect of unreacted PBX 9502 as additional mass or drag on the cylinder wall motion.

2. We use cylinder kinetic energy instead of Gurney energy as it is a more direct measurement which is independent of the copper-explosive mass ratio. This ratio varies with the amount of PBX 9502 IL reaction and thus is not consistent in this experimental configuration.

3. This same issue precludes any analysis of wall motion to yield the product driving pressure and specific volume [1, 12]. Any unreacted PBX 9502 will increase the effective mass to be accelerated radially and result in inaccurate pressure predictions.

The details of our analysis are described below.

5.1. Initiating Layer Mass Fraction

To compute the mass fractions of PBX 9501, IL, and detonating PBX 9502, we use the front shapes shown in Fig. 5 to determine the IL thickness. We then compute the area of each region, using Eqs. 1-3 of [1] to determine the value for the test with the 14 mm core. The resulting mass fractions are shown in Table 3.

5.2. Cylinder Energy

We compute the time-varying CE for each test using the equation

$$CE_T(t) = \frac{V(t)^2}{2}\left(m_w + \left(1 - \frac{ce_{2*}(t)}{ce_2(\infty)}\right)m_{2*}\right) \quad (1)$$

5

Table 3: Properties extracted from the measured front shapes.

Core Diameter (mm)	IL Thickness (mm)	Mass Fraction PBX 9501	Mass Fraction Detonating PBX 9502	Mass Fraction IL
13.5	3.164	0.275	0.396	0.328
14.0	2.645	0.296	0.428	0.276
14.5	3.073	0.318	0.345	0.337

Table 4: Confiner wall velocity fit parameters and CE for $V = V_\infty$.

Core Diameter (mm)	V_∞ (mm/μs)	t_0 (μs)	ω	a_0 (mm/μs^2)	CE (kJ)
13.5	1.576	0.000	1.000	0.807	829
14.5	1.599	-0.001	0.983	0.830	855
PBX 9501	2.054	0.00	0.493	2.256	1276
PBX 9502	1.597	-0.001	0.625	1.604	773

Figure 8: Fitted confiner wall velocity profiles for the annular CYLEX tests.

where CE_T is the total cylinder kinetic energy of an annular CYLEX test, V is the radial wall velocity (which is measured directly by PDV probes oriented normal to the confiner surface), m_w is the mass of the confiner, $ce_{2*}(t)$ is the time-varying, mass-specific cylinder energy contribution from the IL, $ce_2(\infty)$ is the mass-specific cylinder energy from a PBX 9502 CYLEX test at $t = \infty$, m_{2*} is the mass of the initiating layer, and t is time after first wall motion. The expression $(1 - ce_{2*}(t)/ce_2(\infty))m_{2*}$ represents the mass of unreacted PBX 9502 under the assumption it is accelerated to the same velocity as the confiner wall.

The CE for each annular test can also be expressed as the sum of the contributions from each of the layers of Fig 5,

$$CE_T(t) = m_1 ce_1(t) + m_2 ce_2(t) + m_{2*} ce_{2*}(t), \quad (2)$$

where m_1 and m_2 are the masses of detonating PBX 9501 and PBX 9502, and ce_1 is the time-varying, mass-specific cylinder energy from a PBX 9501 cylinder test.

For each test, wall velocity V is calculated as a function of time after first wall motion, t, using an analytic fit to the experimental wall profiles averaged across all PDV probes for each test. The fitting form is

$$V(t) = \frac{V_\infty((t - t_0 + 1)^\omega - 1)}{\frac{2V_\infty\omega}{a_0}(t - t_0 + 1)^\omega - 1} \quad (3)$$

where V_∞, t_0, ω, and a_0 are determined in the fitting process. The fitting is limited to times between 5 and 13 μs after first wall motion in order to avoid the early data where compressible wall motion is apparent and the late data where the PDV traces show evidence of confiner rupture. The parameters determined for the 13.5 and 14.5 mm core tests are reported in Table 4 and the resulting velocity profiles are shown in Fig 8. CYLEX tests for PBX 9501 and PBX 9502 were used to establish CE values as a function of time after first wall motion for each explosive [13, 14]. The values extrapolated to $t = \infty$ are reported in Table 4.

5.3. Degree of Initiating Layer Reaction

To determine the time-varying cylinder energy contribution of the initiating layer, we simultaneously solve

Eqs. 1 and 2 for $CE_T(t)$ and $ce_{2*}(t)$ with $V(t)$ from Eq. 3. These equations are solved at discrete time steps starting at first wall motion, $t = 0$. Then, at each time step, we compute the fraction of mass-specific CE contribution from the initiating layer relative to the CE from detonating PBX 9502. These values are shown in Fig. 9.
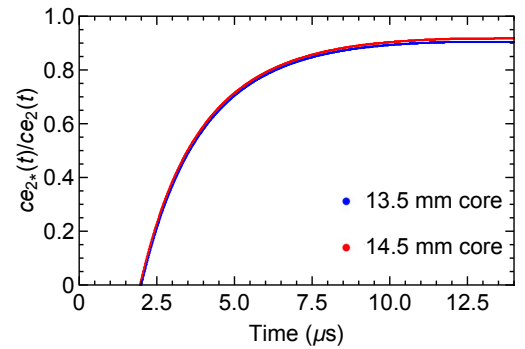

Figure 9: Fraction of mass-specific IL cylinder energy contribution relative to PBX 9502 mass-specific cylinder energy, as measured in a PBX 9502 CYLEX test [14]. Results for the CYLEX test with the 13.5 mm core is shown in blue while the 14.5 mm core test is shown in red.

It should be noted that the curves of Fig. 9 are based on extrapolated $V(t)$ values at times earlier than 5 μs

and later than approximately 13 μs. However, based on the figure, it appears that for both tests, positive energy release by the IL does not occur until approximately 2 μs after first wall motion, and rises quickly until leveling off around 12 μs. By 13 μs, the mass-specific energy release of the IL relative to that observed in a PBX 9502 CYLEX test appears to be around 91% for the 13.5 mm core and 92% for the 14.5 mm core. The slightly lower energy release for the IL in the 13.5 mm core test is consistent with the lower IL shock pressure reported in Table 2.

5.4. Comparison to Prior Results

The annular cylinder test of Hill [1] was nominally of the same dimensions as the tests reported here with the exception of the core diameter of 14.0 mm. The performance of PBX 9501 and PBX 9502 are both dependent on density, but these values are not reported in [1]. However, while the densities of the explosives are not reported directly in that paper, we can compute the density ratio between the two explosives using the reported relationship:

$$\frac{A_1 \rho_1}{A_1 \rho_1 + (A_{2*} + A_2)\rho_2} = 0.296, \qquad (4)$$

where A_1 is the cross sectional area of PBX 9501, A_2 is the cross sectional area of detonating PBX 9502, and A_{2*} is the cross sectional area of the IL. Since $(A_{2*} + A_2)$ is simply the total cross sectional area of PBX 9502, we can use $A_1 = \pi \times 14/2$ and $A_{2*} + A_2 = \pi \times (25.4/2 - 14/2)$. With these values, the ratio between densities must be $\rho_2/\rho_1 = 1.0378$.

Assuming PBX 9501 density of 1.830 g/cc [15], this results in a PBX 9502 density of 1.899 g/cc, which is high relative to the specification of 1.890 +/- 0.005 g/cc. Alternatively, assuming a PBX 9502 density of 1.895 g/cc [15] results in a PBX 9501 density of 1.826 g/cc which is below the minimum specified density of 1.830 g/cc. In any case, the ratio of 1.0378 is quite bit higher than the density ratio of the explosives used in this work, 1.031. We believe this is one reason why the IL metrics of Table 3 show large differences when comparing the 14.0 mm core test of [1] to the other two tests.

Hill [1] also computed a time-varying IL reaction efficiency, but as noted earlier, Gurney energy was used rather than cylinder kinetic energy, drag on the wall motion caused by unreacted PBX 9502 was neglected, and a thermal energy term was included. We believe that these differences in the analysis result in different early time behavior apparent when comparing our Fig. 9 to Fig. 8 of [1]. Furthermore, the early-time compressible motion apparent in the wall velocity profiles makes both Gurney energy and cylinder energy analysis difficult prior to 5 μs after jump, and it is unclear from [1] how this was handled for the 14 mm core test.

In spite of these differences in the method of analysis, the ultimate IL reaction efficiency of 0.86 reported in [1] is quite close to the values we observe in Fig. 9 at 13 μs. The reason for the slightly lower value of [1] may be due to the fact that it does not account for the drag of the unreacted PBX 9502.

6. Conclusions

Two CYLEX tests with explosive charges consisting of a cylindrical PBX 9501 core inside a PBX 9502 shell were performed. The measured front shapes indicated the presence of an IL in the PBX 9502 immediately adjacent to the PBX 9501. A method to analyze the measured wall velocity profiles was developed and used to determine the degree of reaction within the IL. In contrast to prior methods, we consider the mass of unreacted PBX 9502 as drag on the overall system by treating it as additional confiner wall mass. The wall velocity profiles exhibited compressible motion distinct from the typical ringing profiles observed for PBX 9501 or PBX 9502 alone, with three distinct compressible features followed by smooth wall acceleration. Modeling results show negative pressures in the confiner wall, of a magnitude sufficient to result in spall.

Current results were compared to a prior CYLEX test with a similar configuration reported by Hill [1]. The prior test appears to have been conducted with different initial densities for the explosives, possibly leading to the observed differences in the measured front shapes. In spite of this discrepancy and the use of a different method to compute the degree of IL reaction by Hill [1], all three tests indicate a large amount of the PBX 9502 within the IL reacts before confiner wall rupture. The mass-specific energy of the IL appears to reach 86% to 92% of the values measured in PBX 9502 CYLEX tests at 12 - 13 μs after first wall motion. This work thus indicates that while shock deadened PBX 9502 does not detonate promptly, it does eventually react to release a significant portion of its chemical potential energy over longer timescales on the order of 10 μs.

References

[1] L. Hill, Is the detonation "dead zone" really dead?, Proc. Comb. Inst. 35 (2015) 2041–2049.

[2] E. Anderson, T. Aslam, S. Jackson, The Effect of Transverse Shock Propagation on the Shock-to-Detonation Transition Process for an Insensitive Explosive, Proc. Comb. Inst. 35 (2015) 2033–2040.

[3] J. B. Ramsay, A. Popolato, in: 4th Symposium (Int.) on Detonation, Office of Naval Research, 1965, pp. 233–237.

[4] S. A. Sheffield, R. Engelke, R. R. Alcon, in: Ninth Symposium (Int.) on Detonation, Office of Naval Research, 1989, pp. 39–49.

[5] R. L. Gustavsen, S. A. Sheffield, R. R. Alcon, Measurements of Shock Initiation in the Tri-Amino-Tri-Nitro-Benzene Based Explosive PBX 9502: Wave Forms from Embedded Gauges and Comparison of Four Different Material Lots, J. Appl. Phys. 99 (2006).

[6] C. L. Mader (Ed.), LASL Phermex Data Volume III, Los Alamos Series on Dynamic Material Properties, University of California Press, Berkeley, CA, 1980.

[7] W. C. Davis, in: Fourteenth Symposium (Int.) on Detonation, Office of Naval Research, 2010, pp. 1058–1064.

[8] L. Hill, T. D. Aslam, in: Seattle, WA, Presented at the Joint SCCM/AIRAPT Conference, Seattle, WA, 2013.

[9] E. K. Anderson, T. D. Aslam, S. I. Jackson, Transverse initiation of an insensitive explosive in a layered slab geometry: Front shapes and post-shock flow measurements, Combustion and Flame 161 (2014) 1944 – 1954.

[10] C. Matignon, R. Sorin, O. Bozier, in: Fourteenth Symposium (Int.) on Detonation, Office of Naval Research, 2010, pp. 1182–1190.

[11] W. C. Davis, T. R. Salyer, S. I. Jackson, T. D. Aslam, in: 13th Symposium (Int.) on Detonation, Office of Naval Research, 2006, pp. 1035–1044.

[12] S. Jackson, An Analytic Method for Two-Dimensional Wall Motion and Product Isentrope from the Detonation Cylinder Test, Proc. Comb. Inst. 35 (2015) 1997–2004.

[13] S. Pemberton, T. Sandoval, T. Herrera, J. Echave, G. Maskaly, Test Report for Equation of State Measurements of PBX 9501, Technical Report LA-UR-1104999, LANL, 2011.

[14] S. Pemberton, T. Sandoval, T. Herrera, J. Echave, G. Maskaly, Test Report for Equation of State Measurements of PBX 9502, Technical Report LA-UR-1104998, LANL, 2011.

[15] T. Gibbs, A. Popolato, in: LASL Explosive Property Data, University of California Press, 1980, pp. 234–249.

[16] B. Wescott, D. S. Stewart, W. C. Davis, Equation of state and reaction rate for condensed-phase explosives, J. Appl. Phys. 98 (2005) 053514.

[17] M. Short, C. Chiquete, J. B. Bdzil, J. J. Quirk, Detonation diffraction in a circular arc geometry of the insensitive high explosive PBX 9502, Combust. Flame 196 (2018) 129–143.

[18] M. Short, E. Anderson, C. Chiquete, S. Jackson, Experimental and modeling analysis of detonation in circular arc of the conventional high explosive PBX 9501, Proceedings of the Combustion Institute (2020). Submitted.

[19] J. H. Peterson, K. G. Honnell, C. Greeff, J. D. Johnson, J. Boettger, S. Crockett, in: AIP Conference Proceedings, volume 1426, AIP, pp. 763–766.

[20] D. L. Preston, D. L. Tonks, D. C. Wallace, Model of plastic deformation for extreme loading conditions, J. Appl. Phys. 93 (2003) 211–220.

[21] D. E. Burton, Multidimensional discretization of conservation laws for unstructured polyhedral grids, Technical Report, Lawrence Livermore National Lab., CA (United States), 1994.

[22] E. J. Caramana, D. E. Burton, M. J. Shashkov, P. P. Whalen, The construction of compatible hydrodynamics algorithms utilizing conservation of total energy, J. Comp. Phys. 146 (1998) 227–262.